Journal of Applied Polymer Science

Effect of processing conditions on crystallization behavior and mechanical properties of poly(lactic acid) staple fibers

Katharina Bruckmoser,[1] Katharina Resch[1,2]

[1]Materials Science and Testing of Polymers, Montanuniversitaet Leoben, Otto Gloeckel-Strasse 2/II, 8700 Leoben, Austria
[2]Polymer Competence Center Leoben GmbH, Roseggerstrasse 12, 8700 Leoben, Austria
Correspondence to: K. Resch (E-mail: katharina.resch@unileoben.ac.at)

ABSTRACT: Within this study, the applicability of Raman spectroscopy to characterize the crystallinity of PLA staple fibers was evaluated. The influence of the fiber alignment on the possibility to detect crystallinity by using Raman spectroscopy was studied. PLA staple fibers were produced by melt spinning by varying both draw temperature and draw ratio. Systematic interrelationships between the processing parameters of PLA staple fibers and the degrees of crystallinity and the cold crystallization enthalpies were established. Raman spectroscopy showed that the carbonyl stretching band of Raman spectra measured in fiber axis and parallelly polarized was not sensitive to detect crystallinity. However, for perpendicularly polarized measurements, a higher sensitivity was observed. With increasing degree of crystallinity, a reduction of the band width of the normalized carbonyl stretching band was found. The morphology affected the mechanical properties significantly. Increased draw ratio resulted in increased tensile strength and decreased elongation at break. © 2015 Wiley Periodicals, Inc. J. Appl. Polym. Sci. **2015**, *132*, 42432.

KEYWORDS: fibers; morphology; spectroscopy

Received 30 January 2015; accepted 29 April 2015
DOI: 10.1002/app.42432

INTRODUCTION

Poly(lactic acid) (PLA) is a prominent biodegradable and biocompatible polymer, which is produced from renewable resources. PLA can be processed by conventional processing techniques such as injection molding, film extrusion, or melting spinning. Typical applications are packaging elements, medical devices, films, agricultural products, and foams.[1–6] Especially for the textile industry, the production of PLA staple fibers via melt spinning is of great technological interest. Therefore, several studies deal with melt spinning of PLA fibers.[7–13] Especially the draw ratio and the draw temperature were found to have significant effect on the morphology and hence on the mechanical properties of PLA fibers.[7,9,13] Thus, in order to further optimize the application-relevant mechanical properties of PLA fibers, the morphology has to be systematically tailored.

The morphological characteristics such as the degree of crystallinity of PLA are typically characterized by differential scanning calorimetry (DSC).[11,14–19] However, some authors proved a high potential of Raman spectroscopy to distinguish different conformations and different degrees of crystallinity of PLA in the past.[14,20,21] Several authors reported correlations of Raman bands and crystalline morphology in PLA.[14,20–22] Especially, the C=O stretching region in Raman spectrum of PLA is sensitive to conformation and morphology.[20,21] However, only scarce amount of literature is dealing with Raman spectroscopy of PLA fibers.[14] Liao *et al.* investigated the conformation and configuration of PLA nanofibers produced by electrospinning with Raman spectroscopy.[14] However, no comprehensive analysis of crystalline morphology with respect to fiber alignment using Raman spectroscopy was addressed. Furthermore, to the state of knowledge of the authors, no studies dealing with Raman spectroscopy on PLA fibers produced via melt spinning are available.

Thus, this study addresses a comprehensive analysis of the morphology of PLA staple fibers produced via melt spinning. The specific strength of Raman spectroscopy to detect crystallinity and crystalline morphology is evaluated. Raman spectra are correlated with DSC results. Moreover, the effect of morphology on application relevant mechanical properties is discussed.

EXPERIMENTAL

Materials

A conventional PLA fiber grade type 6100D from NatureWorks LLC (NatureWorks LLC, Minnetonka, USA) was used. Prior to processing, the granulate was predried for 7 h at 80°C in vacuum by using a vacuum drying oven (SalvisLab, Rotkreuz, CH).

Fabrication of Staple Fibers

PLA staple fibers were produced by melt spinning on an experimental fiber extrusion line AXON AB (Axon AB Plastics

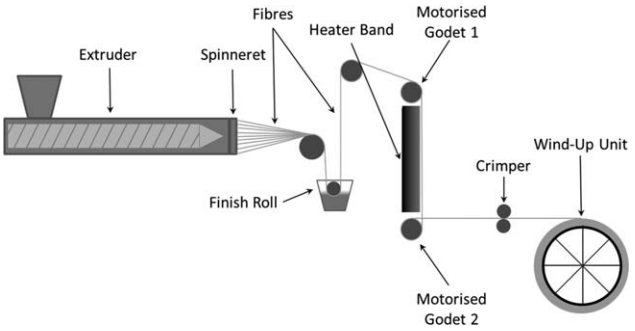

Figure 1. Schematic of the melt spinning line.

Machinery, Nyvång, SE). Figure 1 depicts the schematic of the melt spinning line. Within the extruder, four ascending temperature zones ranging from 198 to 218°C were used. The screw had a diameter of 18 mm and a length of 360 mm. Staple fibers were spun using a spinneret with 375 circular holes with a diameter of 0.7 mm each. Subsequently, a fiber finish based on fatty acids and ethylene oxide was applied. Afterward, drawing of the staple fibers was performed between two motorized and unheated godets (godet 1 and godet 2). Circumferential speed of godet 1 was kept constant at 35 m/min. Circumferential speed of godet 2 was varied to produce different draw ratios. Maximum draw ratios were limited by rupture of staple fibers during stretching. Simultaneously, the staple fibers were exposed to different draw temperatures by using a heater band. Applied draw ratios and draw temperatures are summarized in Table I. Finally, the staple fibers ran through a crimper and were collected on a wind-up unit.

Thermal Analysis

Melting and crystallization characteristics of staple fibers and granulate were measured using a differential scanning calorimeter DSC 1 (Mettler-Toledo AG, Schwerzenbach, CH). The thermograms were recorded under nitrogen atmosphere in a temperature range from 25 to 210°C. The heating rate was 10°C/min. The sample mass was 4.5 ± 0.5 mg. Melting and crystallization characteristics were evaluated from the first heating run according to ISO 11357-3 and subsequently averaged over three measurements. The applied evaluation procedure is presented in Figure 2 schematically. At 60.2°C, the glass transition temperature is detectable. The glass transition is subsequently accompanied by over swinging, which can be attributed to relaxation of orientations which are frozen in a glassy

Table I. Draw Temperatures and Draw Ratios of Produced PLA Staple Fibers

Draw temperature [°C]	23	100	140
Draw ratio [-]	0.99	0.99	0.99
	1.35	1.35	1.35
	1.65	1.65	1.65
	1.95	1.95	1.95
	2.25	2.25	2.25
	-	2.55	2.55
	-	2.85	-

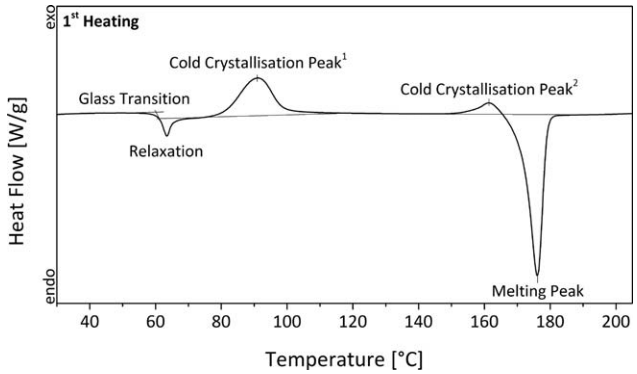

Figure 2. Exemplary DSC curve of first heating of PLA staple fibers.

state.[11,23] After exceeding the glass transition temperature, an increase in the mobility of the polymer chains occurs and glassy polymer chains are transferred into a more stable conformation.[11] The first exothermic peak at 91.2°C is known as cold crystallization peak[1] with cold crystallization enthalpy ΔH_c^1. A second exothermic peak at 161.3°C is referred as *cold crystallization peak*[2] with cold crystallization enthalpy ΔH_c^2. The evaluation of the endothermic melting peak at 176.0°C included the determination of the melting enthalpy ΔH_m and the melting peak temperature. In general, integration limits of cold crystallization enthalpy and melting enthalpy were determined by reaching the level of the baseline. The difference of the melting enthalpy ΔH_m and the sum of the cold crystallization enthalpies ΔH_c^{1+2} is designated as $\Delta H_{m\text{-}c}$. The degree of crystallinity of PLA staple fibers was determined by using eq. (1) where the heat of fusion of 100% crystalline PLA ΔH_0 is 93.1 J/g.[24]

$$\text{Degree of Crystallinity} = \frac{\Delta H_m - \Delta H_c^{1+2}}{\Delta H_0} \cdot 100 = \frac{\Delta H_{m-c}}{\Delta H_0} \cdot 100[\%] \quad (1)$$

Raman Spectroscopy

Raman spectra were recorded on a Labram confocal Raman spectrometer (Horiba JobinYvon GmbH, Bensheim, GER) equipped with a helium neon laser. The line at 632.8 nm with a power of 11 mW was emitted on the sample surface. Raman spectra were recorded in the spectral range of 200–3500 cm^{-1} with a diffraction grating with 1800 grooves/mm and positions of hole and slit of 200 and 100 µm, respectively. An integration time of 4 s with 21 iterations and a 100× objective was used. The fiber alignment was varied in relation to direction of polarization of emitted laser. In Figure 3, the three different fiber alignments are depicted. Raman spectra were measured in fiber axis, parallel to and perpendicular to the direction of the laser polarization. The Raman spectra measured parallelly and perpendicularly polarized were measured on the surface of the staple fibers. Raman spectra recorded in fibers axis were measured in the center of the cross-section. Therefore, fiber samples were embedded in a two-component epoxy resin type EpoThin (ITW Test and Measurement GmbH, Düsseldorf, GER). Afterward, the embedded staple fibers were prepared with a microtome type Reichert Jung (Fa. Reichert Jung, Heidelberg, GER). Recorded Raman spectra were measured in a depth of approximately 3 µm and exhibit a spectral resolution of 1 cm^{-1}. After

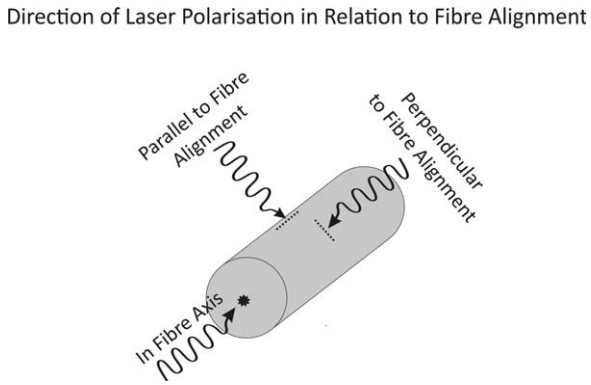

Figure 3. Schematic illustration of directions of laser polarization in relation to PLA staple fibers axis.

a baseline correction using the software LabSpec V.5 (Horiba JobinYvon GmbH, Bensheim, GER), the Raman spectra were normalized to the intensity of C═O stretching vibration of ester groups at 1772 cm^{-1}. Raman spectra were smoothed by applying a Savitzky–Golay filter in Origin 9.0 (OriginLab Corporation, Northhampton, USA).

Fineness Measurement and Tensile Testing

Fineness (titer) of staple fibers was determined on a vibroskop Mod.5 (Lenzing Instruments GmbH and Co KG, Gapern, AUT). Titer was ascertained on 20 staple fibers for each combination of draw ratio/draw temperature. Tensile tests were performed according to DIN EN ISO 5079 on a vibrodyn Mod.5 (Lenzing Instruments GmbH and Co KG, Gapern, AUT). A gauge length of 20 mm and a test speed of 80 mm/min were used. Tests were conducted at room temperature. Tensile strength and elongation at break were averaged over 20 measurements for each combination of draw ratio/draw temperature.

RESULTS AND DISCUSSION

Crystallization and Crystalline Morphology

In Figure 4, the degree of crystallinity determined by DSC is plotted as a function of draw ratio for different draw temperatures. For a draw temperature of 23°C, the degree of crystallinity is hardly affected by the draw ratio. The degree of crystallinity varies between 26 and 31% and reaches a plateau upon increasing draw ratio. This may be attributed to the glass transition of PLA, which is around 60°C. Thus, at a draw temperature of 23°C, the chain mobility is limited. Hence crystallization is hindered. For draw temperatures of 100 and 140°C, the degree of crystallinity increases significantly with increasing draw ratio. Both draw temperatures (i.e., 100 and 140°C) are above the glass transition temperature of PLA. Thus, orientation and chain alignment is facilitated. However, the crystallinity is not significantly affected by the applied temperature level. At a draw temperature of 100°C, the degree of crystallinity varies between 25 and 57% for draw ratios of 0.99 and 2.85, respectively. At a draw temperature of 140°C, the degree of crystallinity varies between 26 and 53% for draw ratios of 0.99 and 2.55, respectively.

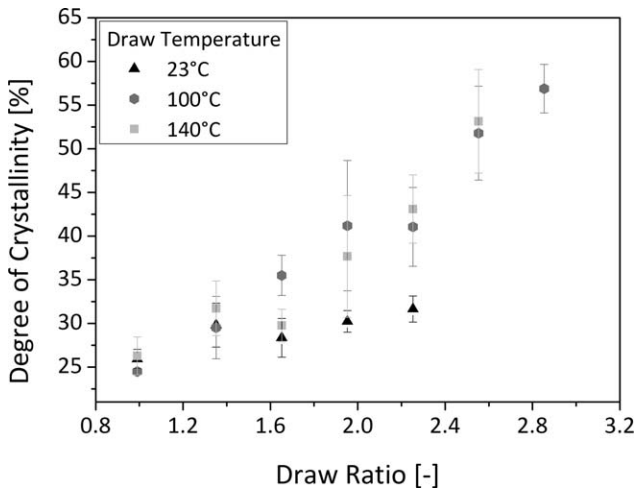

Figure 4. Degree of crystallinity determined by DSC of PLA staple fibers as a function of draw ratio for different draw temperatures.

In Figure 5(a), the cold crystallization enthalpies ΔH_c^{1+2} of PLA staple fibers are presented as a function of the degree of crystallinity for different draw temperatures. Despite the scatter, a distinct interrelationship between ΔH_c^{1+2} and the degree of crystallinity is detectable. High values of ΔH_c^{1+2} provoke low degrees of crystallinity and *vice versa*. This interrelationship is funded in a significant variation of ΔH_c^{1+2} and marginal variation of ΔH_m [cf. Figure 5(b)]. Rapid cooling of PLA staple fibers below the glass transition temperature inhibits the recrystallization. Hence, during heating in DSC above glass transition temperature, cold crystallization occurs[23]. In Figure 6(a), cold crystallization enthalpies ΔH_c^{1+2} of PLA staple fibers are depicted as a function of draw ratio for different draw temperatures. For draw temperatures of 100 and 140°C, H_c^{1+2} decreases with increasing draw ratio. For high draw ratios, less polymer chains are frozen in an amorphous state and the formation of crystals is promoted due to chain orientation. Hence, the cold crystallization is reduced and the degree of crystallinity is enhanced (Figure 4). For a draw temperature of 23°C, ΔH_c^{1+2} is marginally affected by the draw ratio [Figure 6(a)]. As already discussed, this can be ascribed to the reduced mobility of polymer chains and thus reduced formation of crystals during drawing below the glass transition temperature. In Figure 6(b), ΔH_c^1 is presented as a function of ΔH_c^2 for different draw temperatures. Despite the high scatter, a correlation of ΔH_c^1 and ΔH_c^2 is observable. The scatter of ΔH_c^2 can be attributed to slight variations in enthalpy which have a high impact on low values of ΔH_c^2. High values of ΔH_c^1 result in high values of ΔH_c^2 and vice versa. This may be explained by the fact that more material participates in the cold crystallization process (higher ΔH_c^1) after glass transition temperature and thus more material exhibits a loose packing manner.[24] Subsequently, more material transfers to a more stable modification which appears in a higher cold crystallization enthalpy (higher ΔH_c^2) around the melting range.

In Figure 7(a), the effect of draw ratio on the first heating curves of PLA staple fibers at a draw temperature of 23°C is presented. In general, with increasing draw ratio, the relaxation peaks after the glass transition temperature are shifted to higher temperatures and the peak shape changes systematically.

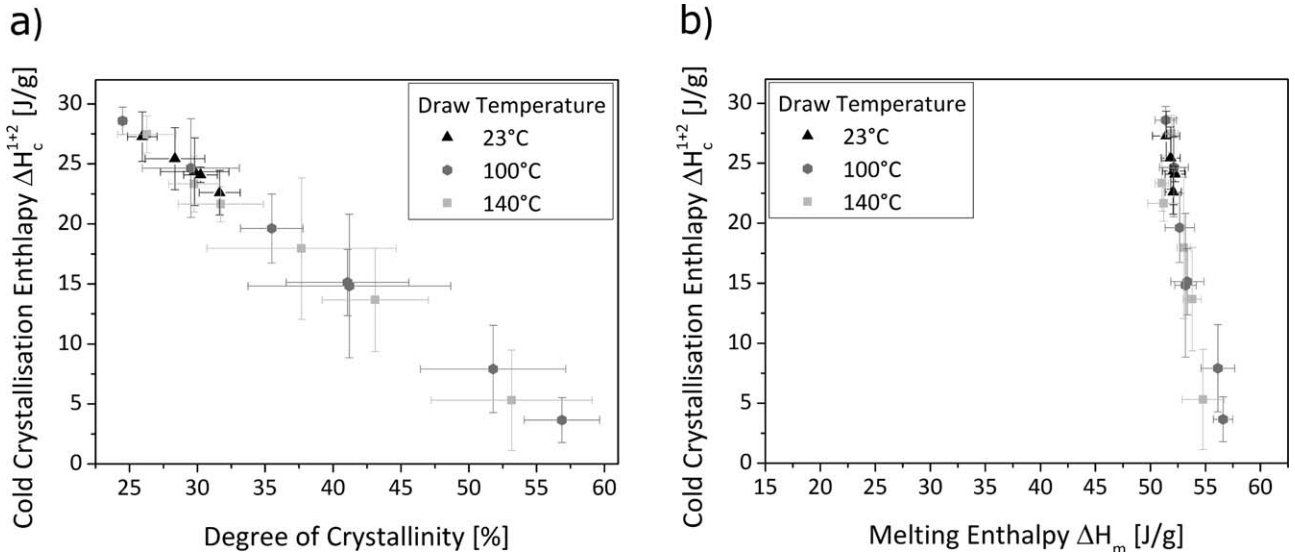

Figure 5. (a) ΔH_c^{1+2} of PLA staple fibers as a function of degree of crystallinity for different draw temperatures (b) ΔH_c^{1+2} of PLA staple fibers as a function of *H*m for different draw temperatures.

However, cold crystallization peaks are marginally affected by the draw ratio (similar cold crystallization enthalpies and similar cold crystallization temperatures). In Figure 7(b), the effect of draw ratio on the first heating curves of PLA staple fibers at a draw temperature of 100°C is depicted. Compared to a draw temperature of 23°C less pronounced endothermic relaxation peaks at glass transition temperature along with continuous changes in peak shapes with increasing draw ratio are ascertainable [cf. Figure 7(a)]. Additionally, the area of the relaxation peak and thus the relaxation process declines with increasing draw ratio. This may be explained by an increased degree of crystallinity at a draw temperature of 100°C compared to draw temperature of 23°C and a lower amount of amorphous fraction with increasing draw ratio. During drawing at temperatures above the glass transition temperature, polymer chains start to form crystals and the amorphous zones are oriented. If rapid cooling below the glass transition occurs, these orientations are frozen. Subsequent heating above the glass transition temperature allows the oriented chains and thus primary amorphous regions to relax. Therefore, a successive reduction of the amorphous fraction with increasing draw ratio yields reduced relaxation phenomena. Moreover, the endothermic relaxation peaks are shifted to higher temperatures with increasing draw ratio. Simultaneously, a reduced cold crystallization enthalpy and a reduced cold crystallization peak temperature as well as a continuous change of the cold crystallization peak shape with increasing draw ratio are observable. This correlation may be explained by a better arrangement of chains in amorphous

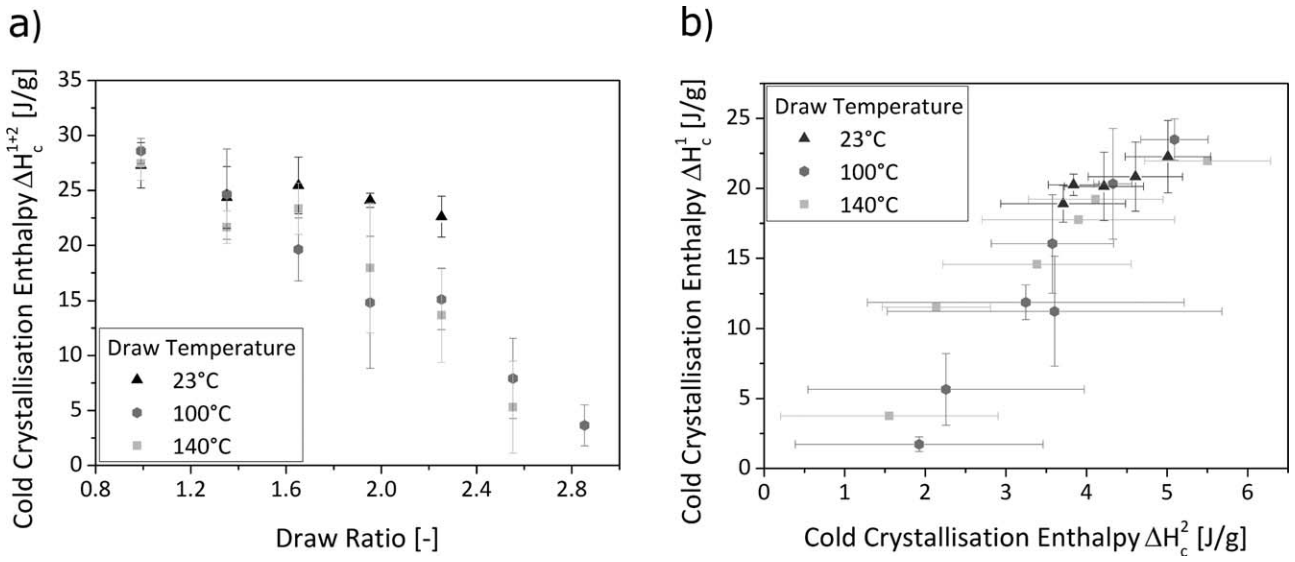

Figure 6. (a) ΔH_c^{1+2} of PLA staple fibers as a function of draw ratio for different draw temperatures (b) ΔH_c^1 of PLA staple fibers as a function of ΔH_c^2 for different draw temperatures.

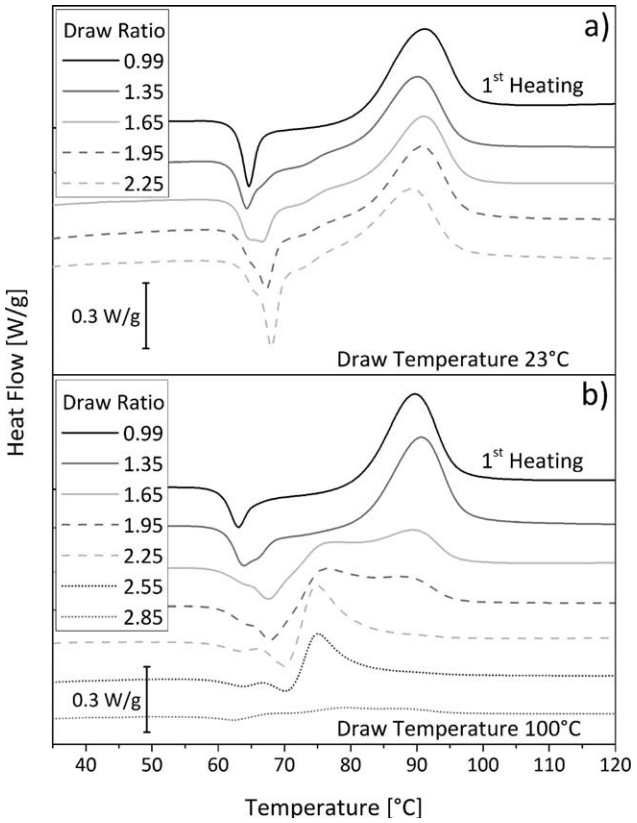

Figure 7. Effect of draw ratio on the first heating curves of PLA staple fibers (a) at a draw temperature of 23°C and (b) at a draw temperature of 100°C.

zones and fewer amounts of amorphous zones when crystallinity is high (increased orientation). Thus cold crystallization is enhanced. Hence, the material reacts faster during heating, since lower temperatures are required to initiate cold crystallization. Similar observations were made by Solarski *et al.*[11]

Interestingly, the melting peak temperatures decrease with increasing degrees of crystallinity (Figure 8). The observed

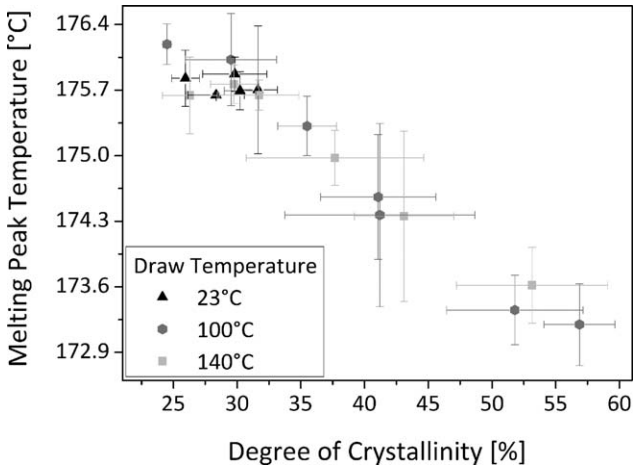

Figure 8. Melting peak temperature of PLA staple fibers as a function of degree of crystallinity for different draw temperatures.

correlation is not influenced by the scatter of the degree of crystallinity. In general, these results indicate a slight decrease of crystal lamellae thickness (lower melting peak temperature) with increasing degree of crystallinity. ΔH_m as a function of the draw ratio for different draw temperatures is presented in Figure 9(a). An increase of ΔH_m with increasing draw ratio is observable. Thus, more crystals are formed at higher draw ratios (orientations). This is associated with a slight decrease of the crystalline order, which is depicted in Figure 9(b), where the melting peak temperatures decrease with increasing draw ratio.

The DSC results clearly show a strong dependence of the morphological characteristics of PLA staple fibers on the processing parameters. In the following, Raman spectroscopy is evaluated as to its specific strength to detect the morphology of PLA staple fibers. Focus is on the crystallinity and the crystalline morphology. However, Raman spectroscopy is sensitive to both orientations and crystallinity. Thus, to exclude the effect of orientations, the effect of different polarization directions in relation to the fiber alignment on the Raman spectra was studied.

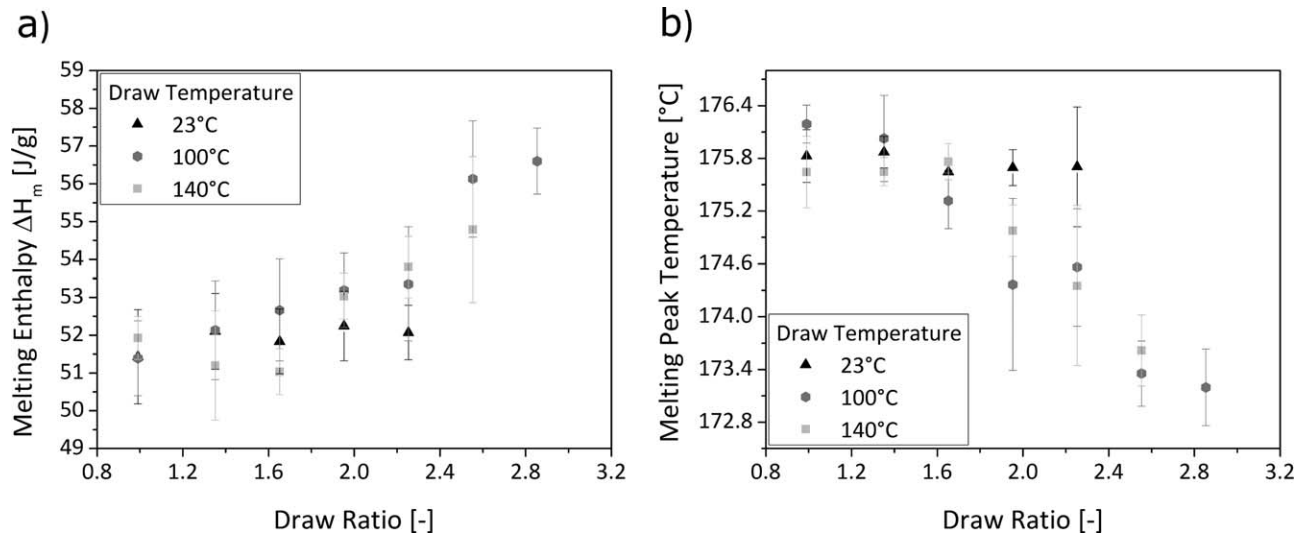

Figure 9. (a) ΔHm and (b) melting peak temperature of PLA staple fibers as a function of draw ratio for different draw temperatures.

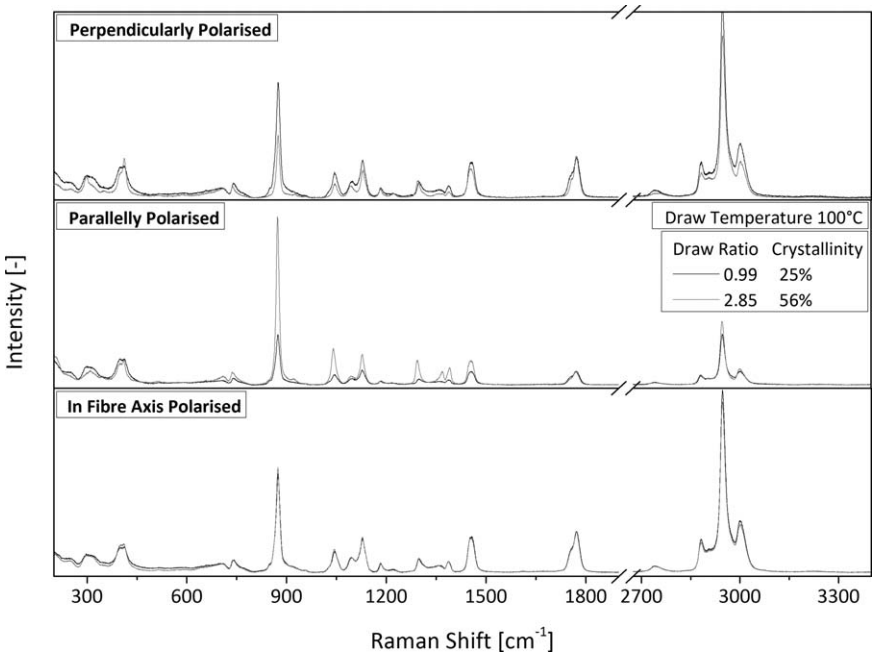

Figure 10. Raman spectra of PLA staple fibers of minimal and maximal draw ratio for different polarization directions.

Therefore, staple fibers at a draw temperature of 100°C and draw ratios of 0.99 and 2.85 were chosen. These samples exhibit the minimum and maximum degrees of crystallinity found in this study. These samples were both measured with perpendicularly, parallelly and in fibers axis polarized laser light (cf. Figure 10). The corresponding assignments of Raman bands are summarized in Table II.

For perpendicularly polarized Raman spectra, the degree of crystallinity affects nearly every Raman band. Similar observations can be made by comparing the Raman spectra measured parallelly polarized. These changes can be ascribed to changes in the degree of crystallinity and orientations. Interestingly, for in fiber axis polarized measurements, nearly coincident Raman spectra are detectable, despite significant differences in the degrees of crystallinity. This clearly indicates that not all polarization directions in relation to fiber alignment show identical sensitivity on the morphology of PLA fibers. Additionally, not every Raman band is sensitive to morphology (e.g., crystallinity and orientations). Especially, the C═O stretching band between 1720 and 1810 cm^{-1} is known to be sensitive to conformation and the degree of crystallinity in PLA.[14,20,21] Thus, this spectral region is presented in Figure 11 in more detail.

In Figure 11, the C═O Raman band of PLA staple fibers of minimal and maximal draw ratio are presented for different polarization directions. The C═O band exhibits a peak at 1772 cm^{-1} and a shoulder at approximately 1753 cm^{-1} which is provoked by a hidden band. For measurements conducted in fiber axis, the band width is hardly affected by the draw temperature and the draw ratio. A slight reduction in band width is observable merely for a draw temperature of 140°C and a draw ratio of 2.55. Parallelly polarized Raman spectra show a slightly reduced band width for maximum draw ratios at draw temperatures of 100 and 140°C. These two samples show significantly higher degrees of crystallinity of 56 and 53% compared to 25 and 26% for minimal draw ratios. Perpendicularly polarized Raman spectra show significantly reduced band widths for maximum draw ratios at draw temperatures of 100 and 140°C. Additionally, the shoulder around approximately 1753 cm^{-1} is more pronounced. Liao *et al.* found similar band shapes in semicrystalline PLA nanofibers.[14] However, Kister *et al.* and Deru and Robert assigned a C═O band with a maximum located at 1768 or 1770 cm^{-1} and a hidden band between 1745 and 1760 cm^{-1} to amorphous PLA.[20,21] In contrast, Kister *et al.* found a sharp tripled band with peaks at 1773, 1763, and 1749 cm^{-1} in semicrystalline PLA.[20] Similar observations were made by Deru and Robert.[21] They assigned a tripled band with sharp peaks at 1776, 1766, and 1750 cm^{-1} to semicrystalline PLA. A more regular chain arrangement and a limited range of bond orientations in semicrystalline PLA are responsible for splitting (crystal field spitting) of the C═O band in semicrystalline PLA. In amorphous PLA, the polymer chains are randomly oriented and all vibrational modes contribute to certain Raman bands.[21] Deru and Robert calculated two Raman intensity ratios of Raman bands at 1776/1770 cm^{-1} and 1766/1770 cm^{-1}. Distinct correlations of intensity ratios and degrees of crystallinity determined by DSC were ascertained. Due to the absence of Raman bands around 1776 and 1766 cm^{-1}, the calculation of this Raman band intensity ratio is not possible within this study.

An exemplary C═O Raman band, the corresponding fitted bands and the fitted spectrum of PLA staple fibers produced at a draw ratio of 0.99 and a draw temperature of 140°C are depicted in Figure 12. The mathematical approximations of the Raman bands are marked with grey color. The slash-dotted grey line represents the sum of the individually fitted peaks and therefore the approximated recorded spectrum. As deducible

Table II. Raman Assignments of PLA (Summarized and Adapted from Refs. 14, 20, 21)

Raman shift [cm^{-1}]	Assignment
3002	Asymmetric stretching CH_3
2947	Asymmetric stretching CH_3
2882	Asymmetric stretching CH_3
1772	Stretching C=O
1454	In-plane asymmetric wagging CH_3
1387	In-plane symmetric wagging CH_3
1295	In-plane bending CH
1182	Stretching OCO
1129	In-plane bending CH_3
1096	Stretching OCO
1045	Stretching C—CH_3
924	Stretching C—C rocking CH_3/Out-of-plane bending CH_3
875	Stretching C—COO
740	Deformation C=O
711	Deformation C=O
412	Deformation C—COO
298	COC + CCH_3

from Figure 12, the C=O peak includes two Raman bands at 1772 and around 1753 cm^{-1}. Based on the individual mathematical approximations, the band widths and the band intensities are available and can be used for quantifying the shape of the carbonyl peak. To quantify the peak width, the full peak width at half maximum (FPWHM) was used. Hence, a comparison of peak characteristics and the corresponding degrees of crystallinity as a function of polarization direction in relation to fiber alignment is possible.

In Figure 13, the degree of crystallinity determined by DSC is correlated with FPWHM of Raman bands at 1753 and 1772 cm^{-1} for different polarization directions. Comparison of FPWHM in fiber axis and parallelly polarized Raman spectra as a function of the degree of crystallinity shows only marginal differences. However, both FPWHM of the C=O band measured

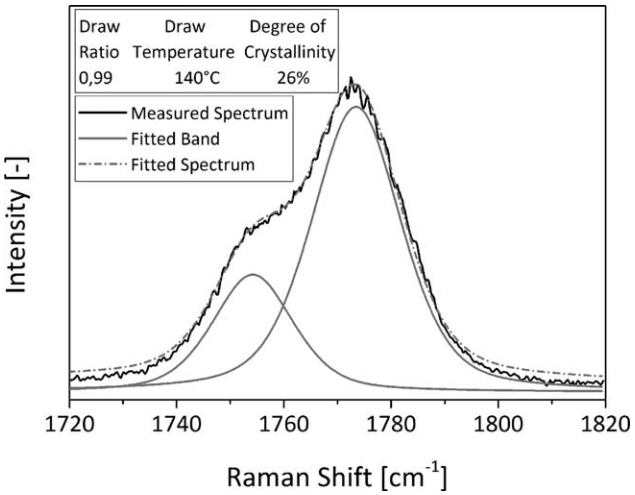

Figure 12. Exemplary Raman spectrum and corresponding fitted bands and spectrum of PLA staple fibers at a draw ratio of 0.99 and a draw temperature of 140°C.

perpendicularly polarized show changes as a function of degree of crystallinity (Figure 13). For high degrees of crystallinity, low FPWHM are detectable and vice versa. FPWHM deduced from measurements performed in fiber axis and parallelly polarized differ only marginally. No distinct correlation between FPWHM and degree of crystallinity is ascertainable. According to Puppulin *et al.*, perpendicularly polarized Raman spectra in relation to fiber alignment are not superimposed by orientations.[25] Thus, the sensitivity to detect crystallinity is maximized. Hence, in the following discussion only spectra recorded perpendicularly to fiber alignment are considered.

Several studies also reported differences in the spectral regions between 1260 and 1410 cm^{-1}, between 810 and 930 cm^{-1}, and between 397 and 411 cm^{-1} by comparing Raman spectra of semicrystalline and amorphous PLA.[14,20,21] In the following, these spectral regions are discussed in more detail.

In Figure 14, the Raman spectra of minimal and maximal draw ratio are depicted for different draw temperatures in the spectral region between 270 and 490 cm^{-1}, 770 and 990 cm^{-1}, and 1250 and 1420 cm^{-1}. High draw ratios yield a reduction in band intensity between 1320 and 1410 cm^{-1}. For maximum

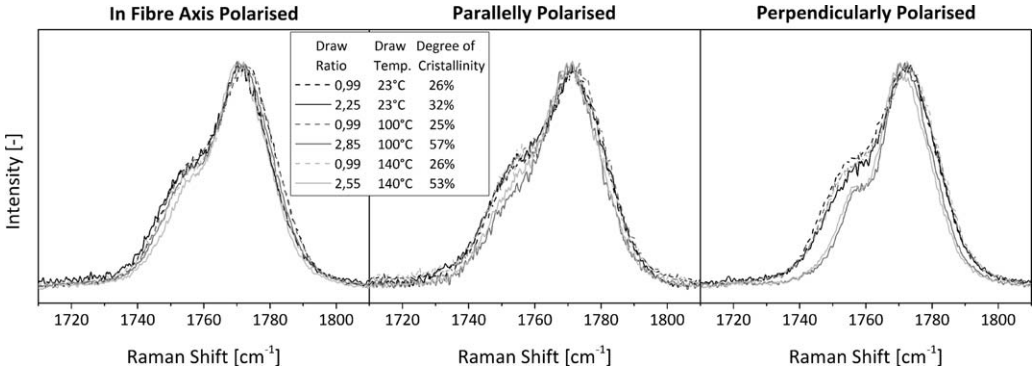

Figure 11. C=O Raman band of PLA staple fibers of minimal and maximal draw ratio for different draw temperatures and different polarization directions.

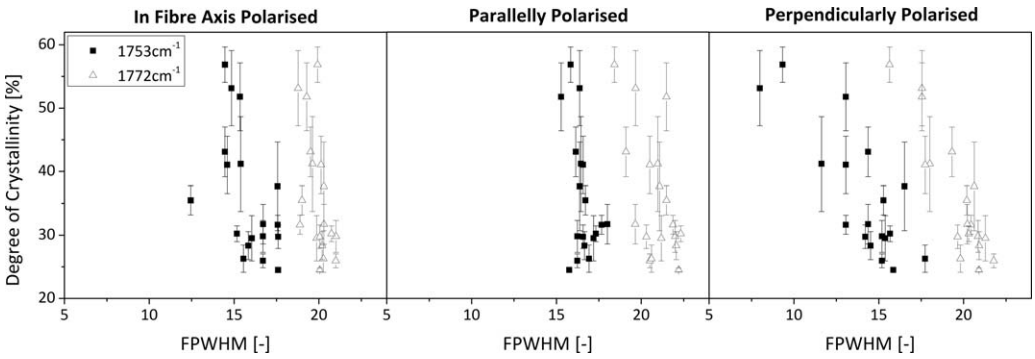

Figure 13. Degree of crystallinity as a function of FPWHM of Raman bands at 1753 and 1772 cm^{-1} for different polarization directions.

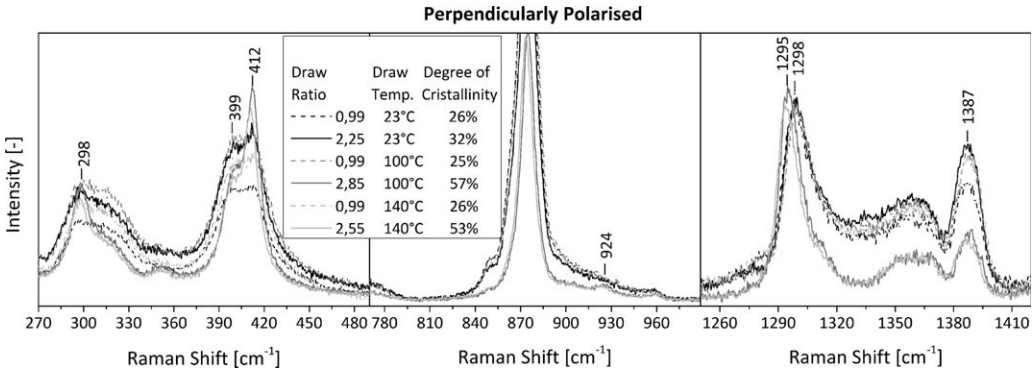

Figure 14. Raman spectra of PLA staple fibers of minimal and maximal draw ratio for different draw temperatures between 270 and 490 cm^{-1}, 770 and 990 cm^{-1}, and 1250 and 1420 cm^{-1}.

draw ratios and draw temperatures of 100 and 140°C, the Raman band at 1298 cm^{-1} shifts to 1295 cm^{-1}. In contrast, no alteration of this band is observable at minimal draw ratios and for a draw temperature of 23°C. A similar peak shift was detected by Kister *et al.* after comparing Raman spectra of amorphous and semicrystalline PLA.[20] However, band splitting was found by Kister *et al.* which was not detectable in this study. A weak band at 924 cm^{-1} is discernible for draw temperatures of 100 and 140°C and maximum draw ratios (Figure 14). This Raman band was detected in semicrystalline PLA at a similar Raman shift of 920 cm^{-1} by Kister *et al.* and was not detected in amorphous PLA.[20] Kister *et al.* ascribed this band to C—C backbone stretching vibrations coupled with CH_3 rocking vibrations.[20] According to Kister *et al.*, this band reflects a 10_3

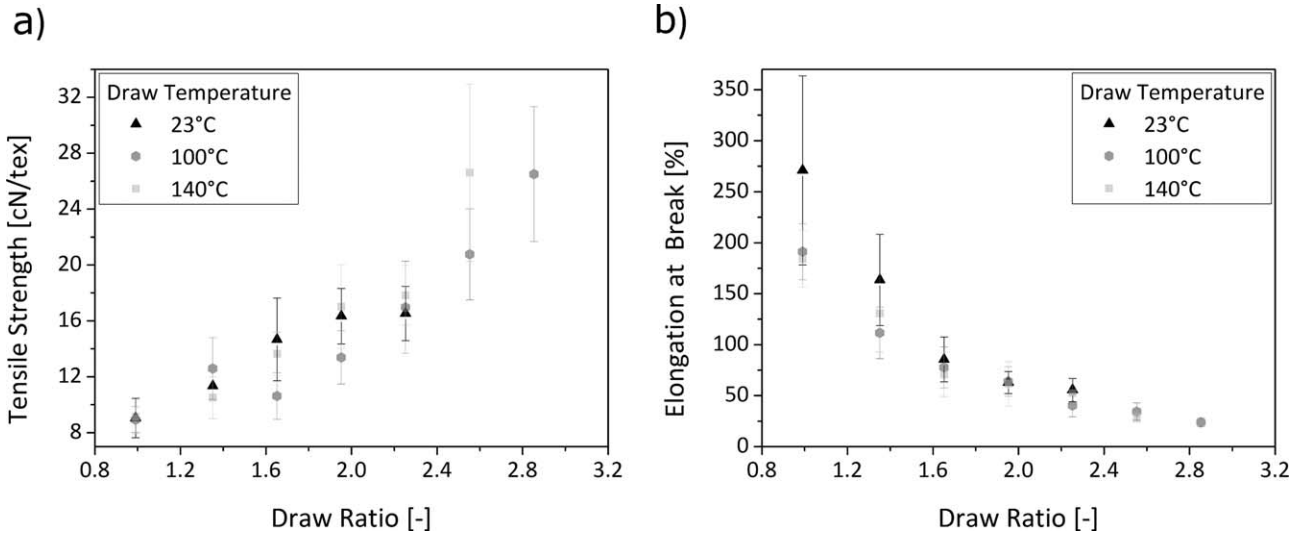

Figure 15. (a) Tensile strength and (b) elongation at break of PLA staple fibers as a function of draw ratio for different draw temperatures.

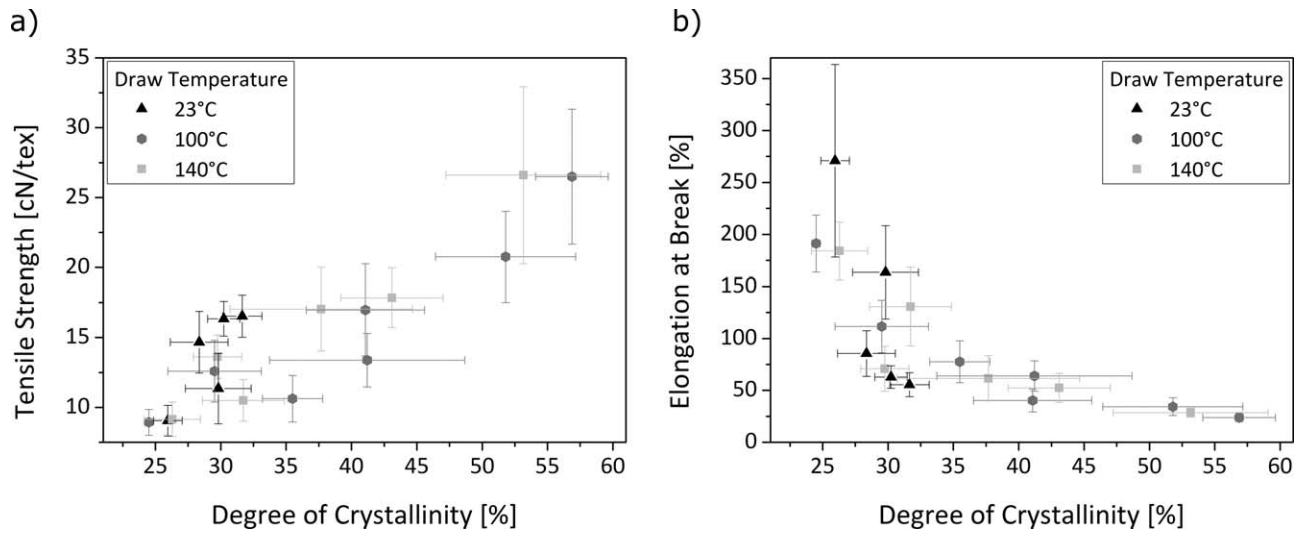

Figure 16. (a) Tensile strength and (b) elongation at break of PLA staple fibers as a function of degree of crystallinity for different draw temperatures.

helix and the presence of this band depends on the type of helical conformation and the crystallinity.[20] In Figure 14, other diversifications in the spectral region of the deformation vibrations of CCO groups and COC groups coupled with CCH_3 groups typically seen at 412 and 298 cm^{-1} are presented.[20] For each draw temperature, a draw ratio of 0.99 yields a double band with peaks at 399 and 412 cm^{-1}. Additionally, a broad band between 270 and 350 cm^{-1} is induced. In contrast, sharp Raman bands at 412 and 298 cm^{-1} appear for draw temperatures of 100 and 140°C at maximum draw ratios. Figure 14 clearly shows that draw temperatures of 100 and 140°C and high draw ratios affect the structure of PLA. The recorded effects are in good agreement with the degree of crystallinity detected by DSC (Figure 4).

Effect of Supramolecular Structure on Mechanical Characteristics

In Figure 15(a), the tensile strength of PLA staple fibers is shown as a function of draw ratio for different draw temperatures. For a minimal draw ratio of 0.99, a tensile strength of 9 cN/tex was measured. A maximum tensile strength of 26.6 cN/tex was achieved for a draw temperature of 140°C and a draw ratio of 2.55. In general, the tensile strength increases with increasing draw ratio. This is due to increased orientations and thus parallel chain alignment. Additionally, it is superimposed by changes in the degree of crystallinity. The scatter in the tensile strength increases with increasing draw ratio. This scatter can be ascribed to defects which yield significantly reduced tensile strengths for staple fibers produced at high draw ratios. Compared to draw temperatures of 100 and 140°C, the tensile strengths of staple fibers drawn at 23°C increase but seem to reach a plateau with increasing draw ratio. Additionally, a draw temperature of 23°C limited the maximum draw ratio to 2.25. Higher draw ratios yielded rupture of the staple fibers. Except the appearance of a plateau at a draw temperature of 23°C, no significant and systematic effect of the draw temperatures on the tensile strength is ascertainable. This indicates that mainly orientations and thus the draw ratio govern the tensile strength. The draw temperature has minor effect on the tensile strength under the investigated conditions. Hence, the effects of orientations superimpose a possible effect of different draw temperatures on the tensile strengths.

In Figure 15(b), the elongation at break of PLA staple fibers is presented as a function of the draw ratio for different draw temperatures. The elongation at break continuously decreases with increasing draw ratio. This can be attributed to increased orientation of polymer chains with increased draw ratio. Hence, maximum elongation of staple fibers is progressively limited. The scatter of the elongation at break simultaneously decreases with increasing draw ratio. This can be ascribed to increasing embrittlement and therefore limited elongation and limited scattering of the elongation of the fibers with increasing draw ratio.

No effect of the draw temperature on the elongation at break is detectable. As already discussed above, this may be attributed to the dominating effect of orientations (draw ratio) compared to the effect of draw temperature on the mechanical properties.

In Figure 16(a), the tensile strength is depicted as a function of the degree of crystallinity for different draw temperatures. The degree of crystallinity scatters as previously presented (cf. Figure 4). However, the observed trend is still significant. High degrees of crystallinity provoke high tensile strengths [Figure 16(a)]. For a draw temperature of 23°C, the degree of crystallinity shows a very high slope between a tensile strength of 11.4 and 16.5 cN/tex. Within the scattering of the tensile strength as a function of the degree of crystallinity, no significant difference between draw temperatures of 100 and 140°C is detectable. This is caused by the likewise increase of the degree of crystallinity and the tensile strength with increased draw ratio for draw temperatures of 100 and 140°C. Similar results can be observed for the elongation at break as a function of the degree of crystallinity in Figure 16(b). Elongation at break is continuously decreasing with increasing degree of crystallinity. Again, no differences

between draw temperatures of 100 and 140°C are observable. This can be attributed to the same effect as discussed above. These results clearly indicate that the tensile properties only depend on the degree of crystallinity (draw ratio) for draw temperatures above glass transition temperature.

CONCLUSIONS

Within this article, the effect of processing conditions on the morphology of PLA staple fibers was characterized by applying DSC and Raman spectroscopy. DSC yielded distinct interrelationships between processing parameters and relaxation, cold crystallization, and melting characteristics during the first heating. The draw temperature and the draw ratio significantly affected the crystallinity. Draw temperatures above the glass transition temperature facilitated higher draw ratios and higher degrees of crystallinity of PLA staple fibers. To optimize the possibility to measure the degree of crystallinity by means of FPWHM of the C═O stretching vibrations at 1753 and 1772 cm^{-1}, Raman spectra have to be recorded perpendicularly polarized. Therefore, Raman spectroscopy proved a high potential to characterize the crystallinity in PLA staple fibers. Moreover, a distinct correlation between fiber morphology and mechanical properties of PLA staple fibers was established. By varying the processing conditions, the morphology and thus the mechanical properties can be tailored. Nevertheless, tailoring of the mechanical properties is restricted because high tensile strengths are inherently associated with low elongations at break and vice versa.

ACKNOWLEDGMENTS

The research work of this article was performed at the Chair of Materials Science and Testing of Polymers at the Montanuniversitaet Leoben and at Asota GmbH. The authors wish to express their gratitude to Dr. Wolfgang Hermann and Mag. Martin Kovac, for providing the sample material, for offering the possibility to produce staple fibers, and for performing mechanical tests.

REFERENCES

1. Auras, R.; Harte, B.; Selke, S. *Macromol. Biosci.* **2004**, *4*, 835.
2. Bianco, A.; Bozzo, B. M.; Del Gaudio, C.; Cacciotti, I.; Armentano, I.; Dottori, M.; D'Angelo, F.; Martino, S.; Orlacchio, A.; Kenny, J. M. *J. Bioact. Compat. Polym.* **2011**, *26*, 225.
3. Geissler, B.; Feuchter, M.; Laske, S.; Fasching, M.; Holzer, C.; Langecker, G. R. *J. Cell. Plast.* **2014**, DOI: 10.1177/0021955X14538274.
4. Ou, X.; Cakmak, M. *Polymer* **2008**, *49*, 5344.
5. Nofar, M.; Park, C. B. *Prog. Polym. Sci.* **2014**, *39*, 1721.
6. Gupta, B.; Revagade, N.; Hilborn, J. *Prog. Polym. Sci.* **2007**, *32*, 455.
7. Cicero, J. A.; Dorgan, J. R. *J. Polym. Environ.* **2001**, *9*, 1.
8. Cicero, J. A.; Dorgan, J. R.; Janzen, J.; Garrett, J.; Runt, J.; Lin, J. S. *J. Appl. Polym. Sci.* **2002**, *86*, 2828.
9. Yuan, X.; Mak, Arthur, F. T.; Kwok, K. W.; Yung, Brian, K. O.; Yao, K. *J. Appl. Polym. Sci.* **2001**, *81*, 251.
10. Fambri, L.; Pegoretti, A.; Fenner, R.; Incardona, S. D.; Migliaresi, C. *Polymer* **1997**, *38*, 79.
11. Solarski, S.; Ferreira, M.; Devaux, E. *Polymer* **2005**, *46*, 11187.
12. Ghosh, S.; Vasanthan, N. *J. Appl. Polym. Sci.* **2006**, *101*, 1210.
13. Furuhashi, Y.; Kimura, Y.; Yoshie, N.; Yamane, H. *Polymer* **2006**, *47*, 5965.
14. Liao, C.-C.; Wang, C.-C.; Chen, C.-Y. *Polymer* **2011**, *52*, 4303.
15. Padee, S.; Thumsorn, S.; On, J. W.; Surin, P.; Apawet, C.; Chaichalermwong, T.; Kaabbuathong, N.; O-Charoen, N.; Srisawat, N. *Energy Procedia* **2013**, *34*, 534.
16. Pegoretti, A.; Fambri, L.; Migliaresi, C. *J. Appl. Polym. Sci.* **1997**, *64*, 213.
17. Schmack, G.; Tändler, B.; Vogel, R.; Beyreuther, R.; Jacobsen, S.; Fritz, H.-G. *J. Appl. Polym. Sci.* **1999**, *73*, 2785.
18. Yuan, X.; Mak, A. F.; Yao, K. *Polym. Degrad. Stab.* **2002**, *75*, 45.
19. Yuan, X.; Mak, A. F.; Yao, K. *Polym. Degrad. Stab.* **2003**, *79*, 45.
20. Kister, G.; Cassanas, G.; Vert, M. *Polymer* **1998**, *39*, 267.
21. Deru, Q.; Robert, T. K. *App. Spectrosc.* **1998**, 488.
22. Kister, G.; Cassanas, G.; Bergounhon, M.; Hoarau, D.; Vert, M. *Polymer* **2000**, *41*, 925.
23. Ehrenstein, G. W.; Riedel, G.; Trawiel, P. In Praxis der thermischen Analyse von Kunststoffen; Hanser: München, **2003**; 17.
24. Lim, L.-T.; Auras, R.; Rubino, M. *Prog. in Polym. Sci.* **2008**, *33*, 820.
25. Puppulin, L.; Takahashi, Y.; Zhu, W.; Pezzotti, G. *J. Raman Spectrosc.* **2011**, *42*, 482.